Journal of Biomedical Optics 9(5), 1103–1109 (September/October 2004)

Automated detection of ocular focus

David G. Hunter
Children's Hospital Boston
Department of Ophthalmology
300 Longwood Avenue
Boston, Massachusetts 02115
E-mail: david.hunter@childrens.harvard.edu

Kevin J. Nusz
Johns Hopkins University School of Medicine
Krieger Children's Eye Center at the Wilmer Institute
Baltimore, Maryland 21287
and
Mayo Clinic
200 First Street Southwest
Rochester, Minnesota 55905

Nainesh K. Gandhi
Imran H. Quraishi
Boris I. Gramatikov
David L. Guyton
Johns Hopkins University School of Medicine
Krieger Children's Eye Center at the Wilmer Institute
Baltimore, Maryland 21287

Abstract. We characterize objectively the state of focus of the human eye, utilizing a bull's eye photodetector to detect the double-pass blur produced from a point source of light. A point fixation source of light illuminates the eye. Fundus-reflected light is focused by the optical system of the eye onto a bull's eye photodetector [consisting of an annulus (*A*) and a center (*C*) of approximately equal active area]. To generate focus curves, *C*/*A* is measured with a range of trial lenses in the light path. Three human eyes and a model eye are studied. In the model eye, the focus curve showed a sharp peak with a full width at half maximum (FWHM) of ±0.25 D. In human eyes, the ratio *C*/*A* was >4 at best focus in all cases, with a FWHM of ±1 D. The optical apparatus detects ocular focus (as opposed to refractive error) in real time. A device that can assess focus rapidly and objectively will make it possible to perform low-cost, mass screening for focusing problems such as may exist in children at risk for amblyopia. © *2004 Society of Photo-Optical Instrumentation Engineers.* [DOI: 10.1117/1.1781669]

Keywords: optics; refractive error; lens opacity; amblyopia; screening.

Paper 03108 received Aug. 19, 2003; revised manuscript received Feb. 12, 2004; accepted for publication Feb. 17, 2004.

1 Introduction

Accurate characterization of the eye's ability to form a high-contrast, focused image is essential in outcome studies of refractive surgery or cataract surgery and when screening for amblyopia. This ''optical performance'' of the eye has been assessed in part by performing visual acuity assessment, refractive error measurement, glare testing, and other studies.[1–4] These studies may require complex optical apparatus, be time intensive, or be highly subjective. Rapid, objective determination of the optical performance of the eye would therefore be valuable in clinical and research settings, including screening for amblyopia risk factors (where the cost and simplicity of screening devices is paramount) and measurement of cataract progression (where traditional photographic and refractive methods are not sufficiently sensitive to nonrefractive factors).

When an eye is looking toward, but is not focused on, a point source of light, a blur patch of light falls on the retina of the eye. Measuring the size of this retinal blur patch would allow determination of the defocus an eye is experiencing.[5,6] We developed a technique using a bull's eye photodetector to characterize the double-pass image of this retinal blur patch automatically. In this paper, we show that this approach can accurately and proportionally measure the retinal blur patch in both model and human eyes, objectively identifying the state of acceptable focus.

2 Materials and Methods

2.1 *Instrument Design*

The critical component of the apparatus is a bull's eye photodetector (Fig. 1) with two concentric active surfaces of nearly equal area, a central circle, and a surrounding annulus. The working hypothesis was that this design could distinguish sharply focused light (falling on only the central area) from defocused light (falling on both the central area and annulus). The surrounding annulus is critical to the design, as a lone photodetector would determine only the intensity of incident room light and would not allow establishment of a single threshold for all eyes. Myopic and hyperopic defocus both increase the size of the blur circle, as do higher order aberrations; all cause a relative increase in light falling on the annulus and thus a decrease in the focus signal.

The detailed design of the focus detection system (FDS) is depicted in Fig. 2. A monochromatic, noncollimated light source (830-nm laser diode) was placed 40 cm from the subject's eye. The distance of 40 cm was selected in anticipation that the device could be used to test children. In our experience, greater distances cause a young subject to lose interest in the target, while lesser distances place the instrument in the proximity of a curious child's reach. A near-IR wavelength was selected to minimize reflex pupillary constriction[7] (and thus loss of signal power). To help isolate the desired reflected signal from background noise, an LDD modulated the LD to create a square wave at 400 Hz.

Horizontal, linearly polarized light diverged from the LD toward a PBS placed approximately 25 cm away. The beamsplitter was oriented to pass all of the horizontally polarized light toward the subject. The light emerging from the beamsplitter was then converted to circularly polarized light using a QWP. The light then passed through a TL and entered the eye. The small amount of light reflected by the fundus maintained most of its circular polarization but changed handedness on reflection, before exiting the eye and returning to the QWP. The reflected light emerged from the QWP vertically

Address all correspondence to David G. Hunter, Children's Hospital Boston, Fegan 4, 300 Longwood Avenue, Boston, Massachusetts 02115. Tel: 617-355-6766; FAX: 617-249-0615; E-mail: david.hunter@childrens.harvard.edu

1083-3668/2004/$15.00 © 2004 SPIE

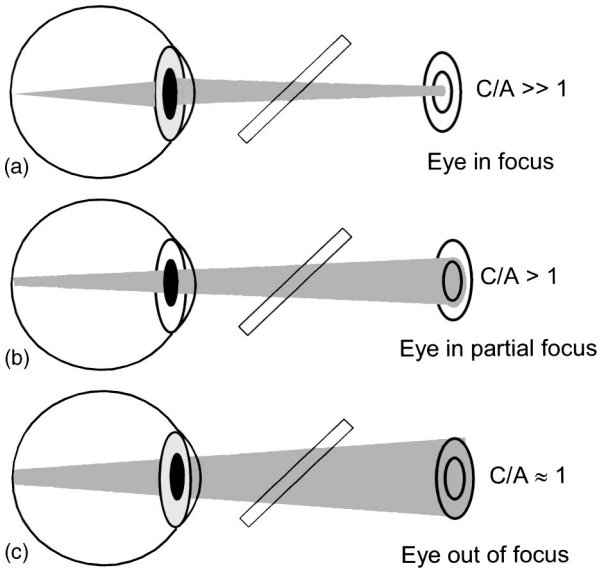

Fig. 1 Representation of light imaged by eye onto bull's eye photodetector: (a) when the eye is in focus, most returning light is imaged onto C, and $C/A \gg 1$; (b) when the eye is partially in focus, more light is imaged onto C than A, and $C/A > 1$; and (c) when the eye is out of focus, returning light is imaged equally onto C and A, and $C/A \approx 1$.

polarized and was deflected toward the photodetector by the PBS.

The circular polarization system was designed to detect maximum light reflected from the fundus while removing half of the depolarized light (produced by facial reflections and other diffuse reflections) from the signal. As a result, any reflected light emerging from the QWP with horizontal polarization, such as that resulting from ocular birefringence, was not deflected toward the detector by the PBS. As long as a substantial fraction of the circularly polarized light reflected from the retina retained its polarization, this optical arrangement maximized the light returning to the bull's eye detector.[8]

The photodetector assembly consisted of the bull's eye photodetector (Silicon Sensor GmBH SSO-KP-6.28-3, Berlin, Germany), a 2.97-mm-diam detector with the central active area having essentially the same total area as the annular active area (central area=3.142 mm^2; annulus area=3.127 mm^2). This size detector at 40 cm, which is calculated to encompass a retinal diameter of 0.12 mm when imaged by a typical eye, provided the best compromise between signal strength and sensitivity.[9] Two photodiode preamplifiers processed the photodetector output, one for each active area of the bull's eye photodiode.

The detectors and LD were aligned in conjugate planes using parallax, then visibly centered under high magnification. Exact optical conjugacy of the point source and detector was essential for proper performance, ensuring that as long as the eye was focused, the retina remained optically conjugate to both.

The detector output was amplified, filtered, and sampled using the analog-to-digital converter on a data acquisition board in a microcomputer running LabView software (National Instruments, Austin, Texas) for analysis. The program displayed the signal of interest and calculated and plotted power spectra of both the center (C) and annulus (A) signals. For each signal, only the component at 400 Hz in the frequency domain was used, thus eliminating artifacts commonly observed at frequencies such as 60 and 120 Hz (including power line noise).

The output of the detectors for individual subjects was plotted as $(C-A)$. The subtraction eliminated any signal that might have been created by diffuse reflection. To adjust for potential differences in overall reflectivity of the eye, which might cause variability in the peak value of $C-A$ for eyes that were equally focused, the ratio C/A was calculated, producing a minimum value of $C/A=1$ for a defocused eye. This

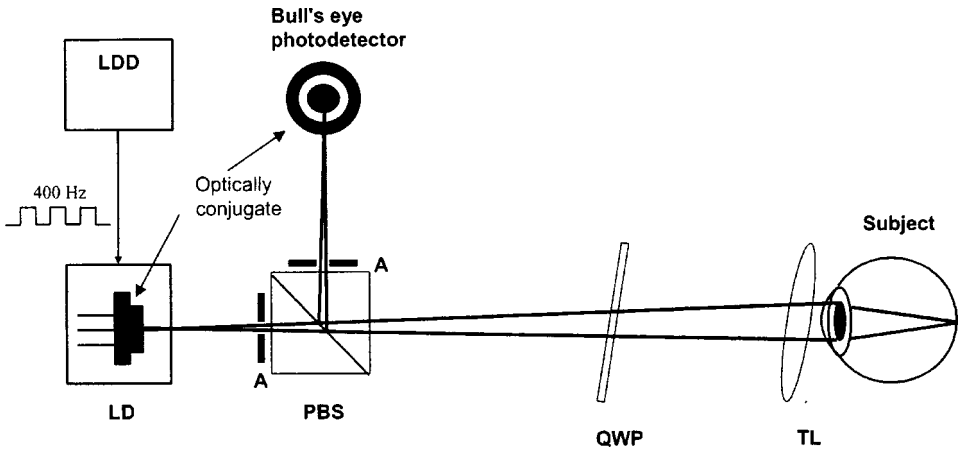

Fig. 2 FDS (viewed from above). The subject is seated adjacent to a lens holder and fixates on an 830-nm laser diode (LD) point source at 40 cm. Linearly polarized light with horizontal orientation [modulated at 400 Hz by a laser diode driver (LDD)] diverges from the point source toward the polarizing beamsplitter (PBS). The emerging light is converted to circularly polarized light by a quarter-wave plate (QWP) before passing through a trial lens (TL) and entering the eye. A portion of the circularly polarized light is reflected from the fundus, where it changes handedness on reflection and returns through the QWP, which converts it to vertically polarized light. The PBS deflects the vertically polarized component of returning light toward the bull's eye photodetector, which is optically conjugate to the point source. To help reduce background noise, apertures (A) are used to limit the light spread from the LD and to limit the acceptance angle of the bull's eye photodetector.

ratio enabled FDS readings to be compared among subjects with varying reflectivity. As the value of A approached zero, the ratio C/A approached infinity. Therefore in some experiments, the normalized ratio $(C-A)/(C+A)$ was calculated. This ratio produced a predictable range of FDS output from 0 for an unfocused eye to 1 for an ideally focused eye.

2.2 *Model Eye Studies*

A model eye (American Optical Corporation), consisting of a single glass lens (simulating the cornea and crystalline lens) with adjustable aperture (simulating the iris) and a movable, flat paper surface (simulating the retina) was used for all model eye studies. Compared with the human eye, the model eye had high reflectivity and low aberration, producing a strong double-pass signal. This model eye was positioned at the location of the subject's eye depicted in Fig. 2. The simulated retina was temporarily replaced with a translucent, IR-detecting film to optimally focus and position the model eye in the system, simulating fixation.

Trial lenses were placed before the model eye to simulate various refractive errors including myopia, hyperopia, and astigmatism. The lenses were tilted 9 deg for the experimental arrangements used for this study to minimize reflections. A plano lens was used when a 0-diopter (D) lens was desired to keep reflections as constant as possible. At least five measurements were obtained for each lens. To determine the influence of pupil size, the internal model eye iris aperture was adjusted prior to obtaining measurements.

2.3 *Human Eye Studies*

All subjects were employees of the Wilmer Eye Institute, Baltimore, Maryland. Informed consent was obtained from all subjects, and the tenets of the Declaration of Helsinki were followed. The Johns Hopkins Institutional Review Board approved the study procedures. Safe light levels[10] were used at all times.

An ophthalmologist (DLG or DGH) measured the refractive error of subjects using standard clinical techniques. Spherical trial lenses bracketing the point of best focus by ± 5 D in 0.25- or 0.50-D increments were then selected. The smaller increments were used closer to the point of best focus.

For each measurement session, a background signal was obtained with the subject positioned in front of the apparatus with eyes closed. This signal, which measured internal reflections in the apparatus, was subtracted from all subsequent measurements to improve the SNR. For any experimental arrangement used in this study, the background signal varied by less than 5%. Pupil area was measured in ambient lighting conditions using an image capture system with a coaxial, near-IR light source.

The subject was seated at the apparatus, with the eye positioned behind the desired lens, and was asked to gaze toward the point source. The monochromatic, near-IR point source was readily visible to observers as a moderately intense spot of red light. Subjects had no difficulty judging when the point source appeared to be in best focus. Younger subjects were encouraged to avoid accommodation by looking toward but not focusing on the blurry point source of light. The subject then depressed a button to record a focus detection measurement. Each measurement was obtained in less than 0.2 s. At least five measurements were obtained and averaged for each trial lens. To maintain tear film integrity, the subject was asked to blink between each measurement.

To determine the effect of pupil size on the focus curve profile, the pupil was constricted or dilated using pharmacologic manipulation. For constriction, a drop of 1% pilocarpine was administered. Focus curves were generated at intervals after maximum constriction as the pupil returned to its native size. For dilation, a drop of 1% tropicamide was administered, and focus curves were generated at intervals as the pupil returned to its native size.

3 Results

3.1 *Model Eye Focus Curves*

The signals obtained from the center (C) and annulus (A) of the bull's eye photodetector using the model eye are shown in Fig. 3(a). As the defocus increased in either the myopic or hyperopic direction, C decreased, while A simultaneously increased, consistent with spread of defocused light over a wider area of the detector. This is further characterized in Fig. 3(b), illustrating the differential signal magnitude at various levels of spherical defocus. The shape of the combined signal $C-A$ obtained from the model eye was similar to the shape of the center signal (C) due to the minimal scatter of light at best focus. At greatest defocus, the amplitude of C was nearly equal to the amplitude of A, so that $C-A$ approached zero. The peak value had a full width at half maximum of ± 0.25 D.

3.2 *Human Eye Focus Curves*

A representative sample of the time-based, subtracted output of $C-A$ obtained from a human eye is shown in Fig. 4. The 400-Hz carrier signal is evident in Fig. 4 whether the eye is in or out of focus. The signal amplitude increased when the eye was in focus. A typical focus curve of a human eye is shown in Fig. 5 for a presbyopic, nonaccommodating subject. The peak in this curve, located at approximately $+1.25$ D, is located where the point source appeared to be in best focus according to the observations of the subject. The point of best focus was shifted to the right due to chromatic aberration of the eye for near-IR light relative to the eye's refraction for the test distance in white light.

The change in the strength and profile of the focus curve obtained from this human eye as pupil size varied is illustrated in Fig. 6. With decreasing pupil area, overall signal power decreased, with a corresponding broadening of the peak. A slight hyperopic shift was also observed. With larger pupil area, overall signal power was increased, but the shapes of the focus curves remained similar, and no myopic or hyperopic shift was observed. A similar relationship between signal strength and aperture size was observed in the model eye, except that no myopic or hyperopic shift was observed.

The focus profile using C/A is shown for four eyes of three subjects in Fig. 7. The curves have been shifted horizontally to place the peak values at zero defocus for comparison purposes. The ratio C/A was >4 in all cases when the proper corrective lens was introduced, and the width of the focus curve was about ± 1 D at half maximum. From this analysis, $C/A \geqslant 4$ was considered a candidate threshold of acceptable focus (Fig. 7, horizontal line.) Nearly identical curve shapes

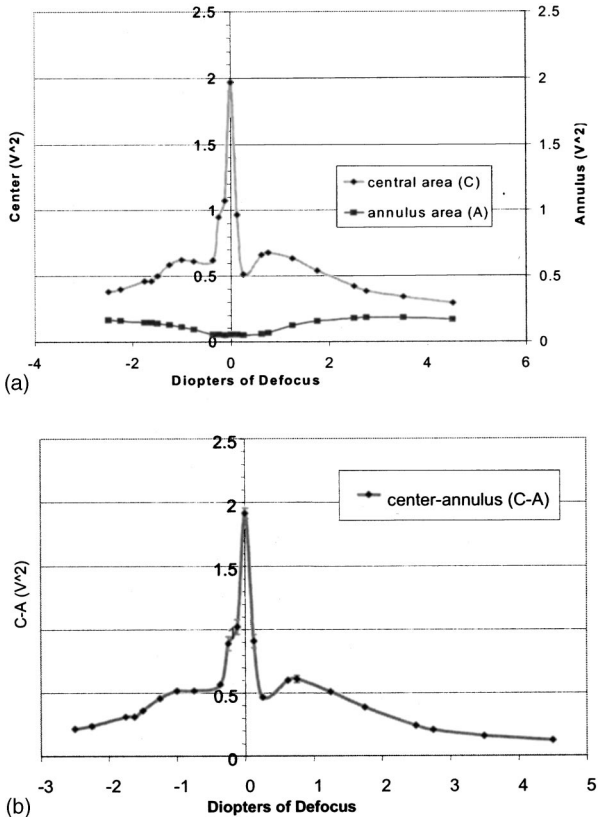

Fig. 3 Focus detection curves (model eye): (a) signal voltage obtained from the center (*C*) and the annulus (*A*) of the bull's eye photodetector, plotted as a function of the change in focus of the model eye, and (b) the magnitude of the differential signal $(C-A)$ at various levels of spherical defocus illustrated by plotting $C-A$ measurements as a function of defocus (in diopters). The full width at half maximum of the peak is ±0.25 D.

were observed when the normalized ratio, $(C-A)/(C+A)$, was calculated.

3.3 *Astigmatic Eyes*

Planocylindrical lenses ranging from plano (0 D) to +3 D were placed in front of the model eye, and focus curves were generated for each lens. As cylinder power increased, the cross-sectional profile of the focus curve decreased in overall height and also developed a double peak that straddled the point of zero spherical power. The separation between peaks increased proportionally with increased cylindrical power. The focus curve of astigmatic human eyes showed alterations similar to those observed in the astigmatic model eye (Fig. 7, subject 1, OD).

4 Discussion

If a point source of light is not focused onto the retina, the double-pass image should be proportional in diameter to the retinal blur circle.[5,6,11] Measuring the size of the double-pass image of a point source should thus determine the goodness of image focus. A procedure to measure light spread of the optics of the eye using a double-pass image of a slit of light was introduced in 1955 by Flamant.[12] This approach was subsequently modified to utilize a point source of light.[13] Advances in the quality of charge-coupled devices allowed better characterization of this double-pass image.[14,15] In 1994, Westheimer and Liang[5] developed a system using an ultrasensitive charge-coupled-device camera to create an ''index of light diffusion,'' where light was measured in separate but unequal central and annular zones. Elliott and Mickelson[16] had previously developed and patented a system to detect focused light using central and annular photodetectors, also of unequal area. Their focusing system was devised specifically for a videodisk reading system to ensure that the scanning beam was always focused precisely at the videodisk.

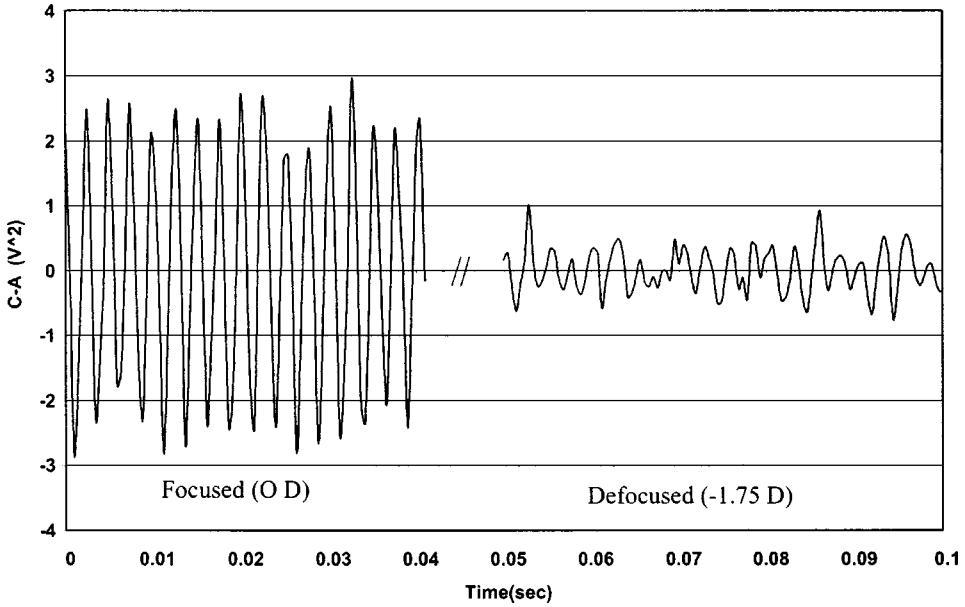

Fig. 4 Representative FDS signal from human eye: time-based sample of differential signal $(C-A)$ measurements as a function of time (in seconds). Whether the eye is in or out of focus, the 400-Hz carrier signal is evident. Signal amplitude, however, changes with focus, with an increase in the focused state and a decrease when the eye is out of focus.

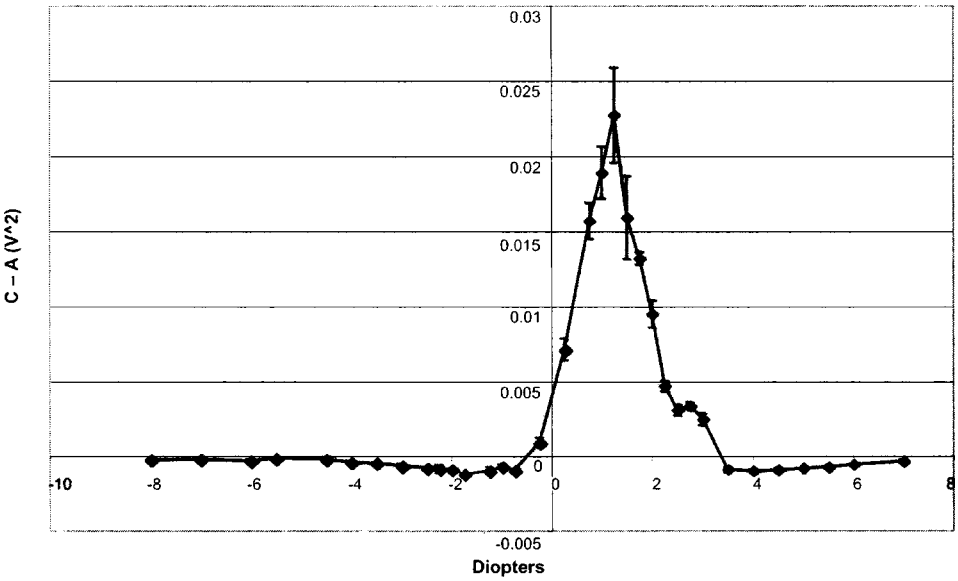

Fig. 5 Focus curve for a representative human eye: differential signal ($C-A$) measurements obtained from a presbyopic, nonaccommodating subject plotted as a function of defocus (in diopters). The curve peak (approximately +1.25 D) matched the point of subjective best focus.

Guyton et al.[17] combined Westheimer's concept of measuring the double-pass image of a point light source produced by the eye with Elliott's concept of utilizing a simple, dual-area, concentric detection system to assess the state of focus. Specifically, they described the concept of using a bull's eye photodetector, consisting of a center (C) and annulus (A), to assess the size of the blur patch of the eye. This approach is unique in that it determines when the blur patch exceeds a particular threshold without need for subsequent image analysis. This is simpler and less expensive than approaches that use a camera to produce (and a computer to characterize) the double-pass image. The use of a small center, and an annulus of equal area, further simplifies differential detection by automatically excluding unfocused or scattered light from the differential signal.[17] The purpose of this study was to determine whether such an approach could be used to characterize the focus of the eye in human subjects.

The focus detection system produced a maximum signal at the point of best focus in both the model eye [Fig. 3(b)] and the human eye (Fig. 5). The signal obtained from the model eye was superior to the signal obtained from the human eye, with higher power and sharper focus curves. This was anticipated due to the more efficient single reflective layer of the model eye, the increased precision of the fixed focus of the model eye, the imperfect optics of the human eye (including spherical aberration and coma), and the possible reduction in

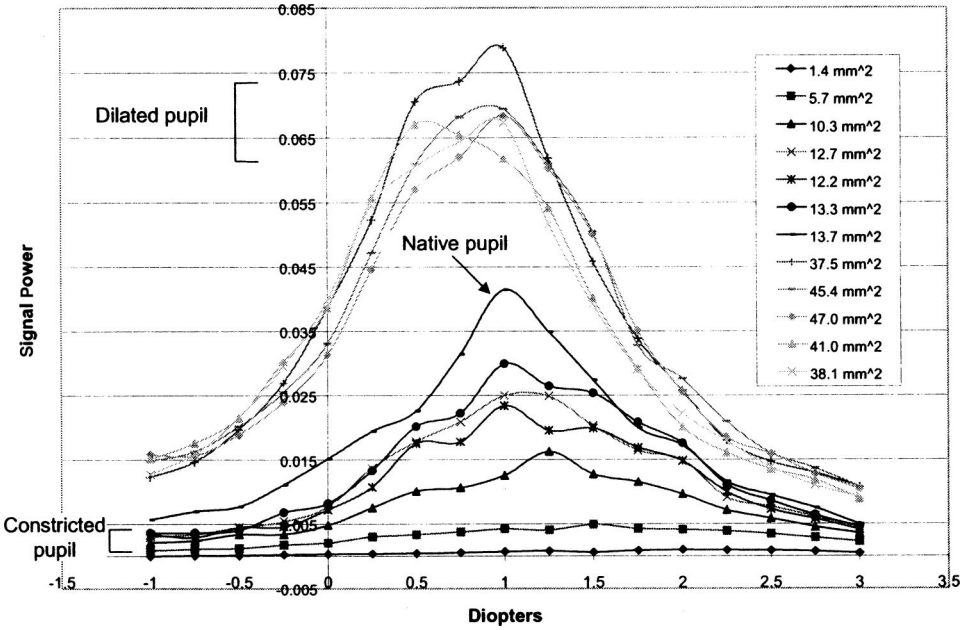

Fig. 6 Dependence of signal power on change in pupil area in a representative subject.

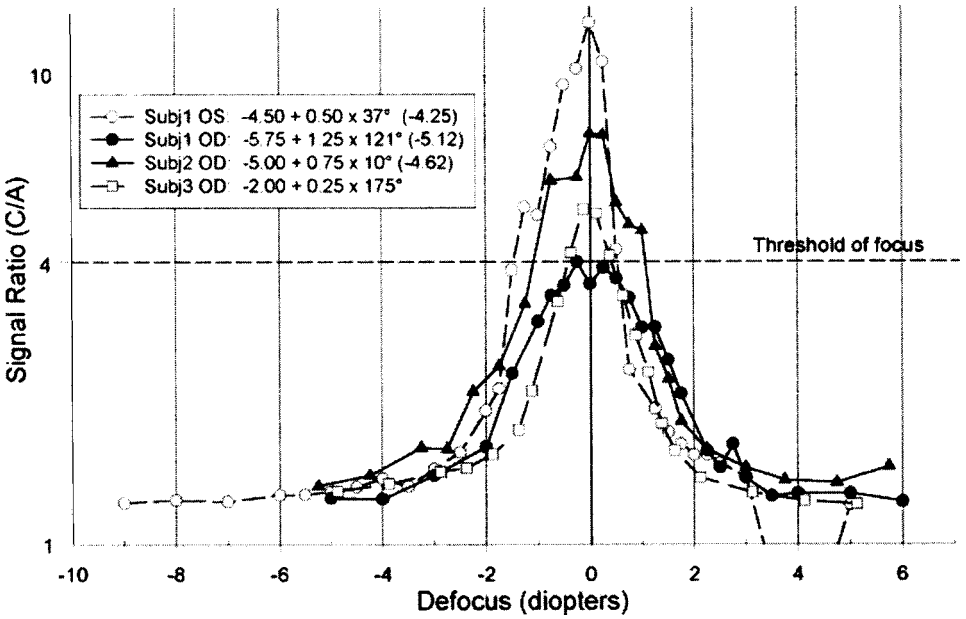

Fig. 7 FDS focus profiles from four human eyes, centered about zero defocus: the signal ratio (C/A) was plotted as a function of defocus (in diopters). To adjust for potential differences in overall reflectivity of the eye, which might cause variability in the peak value of $C-A$ for eyes that were equally focused, the ratio C/A was calculated; OD, right eye; OS, left eye.

SNR caused by reflections from the face and other surfaces around the human eye. In addition, subjects 1 and 2 had normal accommodation, and while procedures were utilized to minimize any variability from accommodation, such variability would have broadened the peaks.

Focus profiles obtained for human eyes had a signal ratio of >4 for the focus peak and a full width at half maximum of approximately ± 1 D for all four volunteer eyes. This indicates that the system, if set at a fixed threshold for all subjects, has the potential to detect spherical focus within ± 1 D. A higher threshold produces a narrower range of acceptable focus but might exclude focused eyes that produce a lower but otherwise-adequate signal.

In the pupil size experiments, the focus curves became broader as the pupil size decreased in the both human and model eyes. A smaller pupil increases the depth of focus, which decreases the alteration in the double-pass image caused by defocus, thus producing a broader focus curve. A larger pupil decreases the depth of focus and narrows the focus curve slightly, with further narrowing limited by the size of the detector. The pharmacologic agents used to manipulate pupil size may have affected the location of the peak of the focus curves through action on accommodation but should not have affected the magnitude of the peak.

In astigmatic eyes, the focus curve consisted of a depressed double peak, the separation of which was proportional to the amount of astigmatism present. This double peak was predicted by mathematical modeling of the extended conoid of Sturm produced by an astigmatic double-pass point source image (Fig. 8) and overlaying this cross section onto the bull's eye pattern. The astigmatic elliptical or line-shaped double-pass image falls at least partially onto both the center and annulus of the bull's eye detector, producing a partially defocused FDS signal. The predictions of the model were consistent with the observation of a focus profile with two peaks from subject 1 OD (Fig. 7), who had an astigmatic error of 1.25 D. Smaller amounts of astigmatism were not detected with the bull's eye detector diameter used in this study, but this is not likely to be an important limitation, as astigmatism of less than 1.25 D is not believed to increase the risk for conditions such as amblyopia.

The results of this study indicate that the FDS can be used to identify eyes that produce acceptably focused images, without regard to traditional refractive error measurements. For example, our laboratory used the FDS to characterize cataract-induced blur.[18,19] In that study, the FDS curves after cataract surgery were taller and narrower, and contained more light energy.

The simplicity of the FDS is desirable considering its potential application of mass screening of patients for acceptable focus, such as screening of pediatric patients at risk for am-

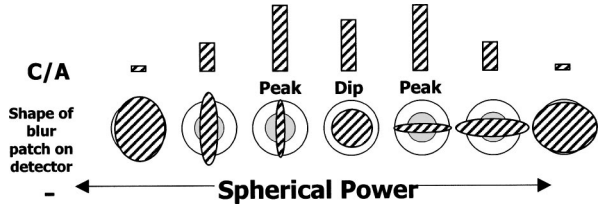

Fig. 8 Extended conoid of Sturm projected onto the bull's eye photodetector: mathematical model representing cross sections of the extended double-pass conoid of Sturm, produced by an astigmatic eye of a point source of light, overlaid onto the bull's eye pattern. The elliptical or line-shaped astigmatic double-pass images fall onto both the center and annulus of the bull's eye photodetector, producing at best partially defocused FDS signals. The corresponding FDS signals (C/A) are represented above the astigmatic blur images, with even the peak signals depressed somewhat compared with those from sharply focused spherical images.

blyopia. Spherical defocus, astigmatism, or other optical irregularities will decrease the signal. The in-focus state can be detected automatically, in near real time, without the necessity of expert interpretation or cycloplegia. While more expensive or elaborate approaches have been used to measure refractive error, the simplicity of the FDS will minimize the cost, weight, and complexity of such a screening device.

The dependence on the accommodative status of the eye may at first appear to be a disadvantage of the FDS, but for future screening applications this feature actually provides an advantage over measurements of distance refractive error. For example, a hyperopic eye that is compensated by accommodation will not become amblyopic and will pass the FDS screening because the signal will be strong. But if accommodation is faulty, then the eye may already be amblyopic or may become amblyopic, and this will be detected in the FDS screening by a weak signal. If, however, the accommodative effort induces strabismus, a second system to detect eye misalignment simultaneously will be required.

The magnitude of the FDS signal represents a single threshold of focus that the eye must achieve to indicate that no abnormalities, whether accommodative, refractive, or media opacity, are interfering with the image-forming ability of the eye. The FDS may thus represent a novel approach to automated vision screening. However, the achievable parameters of sensitivity and specificity must still be determined.

Acknowledgments

The authors thank David Kays for assistance with equipment fabrication. Grant support provided by: Research to Prevent Blindness [Lew R. Wasserman Merit Award (DGH)], (DLG), the National Institutes of Health (NIH) EY-12883 (DGH), the Massachusetts Lions Eye Research Fund, Inc. (DGH), the Roy and Niuta Titus Foundation (DGH), the Helena Rubinstein Foundation (DGH), the Alcon Research Institute (DLG), and the Thomas Wilson Sanitarium (DLG).

References

1. D. Elliot, ''Evaluating visual function in cataract,'' *Optom. Vision Sci.* **70**, 896–902 (1993).
2. G. S. Rubin, I. A. Adamsons, and W. J. Stark, ''Comparison of acuity, contrast sensitivity, and disability glare before and after cataract surgery,'' *Arch. Ophthalmol. (Chicago)* **111**, 56–61 (1993).
3. G. R. LaRoche, ''Amblyopia: detection prevention, and rehabilitation,'' *Curr. Opin. Ophthalmol.* **12**, 363–367 (2001).
4. E. E. Hartmann, V. Dobson, L. Hainline, W. Marsh-Tootle, G. E. Quinn, M. S. Ruttum, P. P. Schmidt, and J. Simons, ''Preschool vision screening: summary of a task force report,'' *Ophthalmology* **108**, 479–486 (2001).
5. G. Westheimer and J. Liang, ''Evaluating diffusion of light in the eye by objective means,'' *Invest. Ophthalmol. Visual Sci.* **35**, 2652–2657 (1994).
6. M. Karbassi, P. C. Magnante, J. K. Wolfe, and L. T. Chylack, ''Objective line spread function measurements, Snellen acuity, and LOCS II classification in patients with cataract,'' *Optom. Vision Sci.* **70**, 965–962 (1993).
7. N. Lopez-Gil and P. Artal, ''Comparison of double-pass estimates of the retinal-image quality obtained with green and near-infrared light,'' *J. Opt. Soc. Am. A* **14**, 961–971 (1997).
8. G. J. van Blokland, ''Ellipsometry of the human retina in vivo: Preservation of polarization,'' *J. Opt. Soc. Am. A* **2**, 72–75 (1985).
9. N. K. Gandhi, ''Determination of ocular defocus using the double-pass blur image of a point source of light,'' Master's Thesis, Johns Hopkins University (2000).
10. D. Sliney and M. Wolbarsht, ''Current laser exposure limits,'' in *Safety with Lasers and Other Optical Sources*, pp. 261–283, Plenum, New York (1980).
11. E. Hecht and A. Zajac, *Optics*, 2nd ed., pp. 270–326, Addison-Welsey Publishing Co., Reading, MA (1987).
12. F. Flamant, ''Étude de la repartition dans l'image rétinienne d'une fente,'' *Rev. Opt., Theor. Instrum.* **34**, 433–459 (1955).
13. A. Arnulf, J. Santamaria, and J. Bescos, ''A cinematographic method for the dynamical study of the image formation of the human eye,'' *J. Opt. Soc. Am. A* **12**, 123–128 (1981).
14. J. Santamaria, P. Artal, and J. Bescos, ''Determination of the point-spread function of human eyes using a hybrid optical-digital method,'' *J. Opt. Soc. Am. A* **4**, 1109–1114 (1987).
15. R. Navarro, P. Artal, and D. R. Williams, ''Modulation transfer of the human eye as a function of retinal eccentricity,'' *J. Opt. Soc. Am. A* **10**, 201–212 (1993).
16. J. E. Elliott and L. Mickelson, ''Optical transducer and focusing system,'' U.S. Patent No. 4,152,586 (May 1, 1979).
17. D. L. Guyton, D. G. Hunter, J. M. Masters, S. N. Patel, and R. L. Fry, ''Eye fixation monitor and tracker,'' U.S. Patent No. 6,027,216 (Feb. 22, 2000).
18. K. J. Nusz, N. G. Congdon, T. Ho, B. I. Gramatikov, D. S. Friedman, D. L. Guyton, and D. G. Hunter ''Rapid objective detection of cataract-induced blur using a bull's eye photodetector,'' *J. Cataract Refractive Surg.* (in press).
19. A. J. Roorda, ''Double-pass reflections in the human eye,'' Ph.D. Thesis, University of Waterloo, Ontario, Canada (1996).